

Influence of Nitrate and Phosphate on Silica Fibrous Beta Zeolite Framework for Enhanced Cyclic and Noncyclic Alkane Isomerization

Siti Maryam Izan, Aishah Abdul Jalil,* Che Ku Nor Liana Che Ku Hitam, and Walid Nabgan



Cite This: <https://dx.doi.org/10.1021/acs.inorgchem.9b02914>



Read Online

ACCESS |



Metrics & More



Article Recommendations



Supporting Information

ABSTRACT: Phosphate and nitrate were loaded on silica BEA (P/HSi@BEA and N/HSi@BEA), which is fibrously protonated by the impregnation method for *n*-hexane and cyclohexane isomerization. The characterization analysis specified the removal of tetrahedral aluminum atoms in the framework, which was triggered by the existence of phosphate and nitrate groups in the catalyst. The exchanged role of Si(OH)Al to P–OH as active acidic sites in the P/HSi@BEA catalyst reduced its acidic strength, which was confirmed by the FTIR results. Lewis acidic sites of P/HSi@BEA performance are a significant part in the generation of high protonic acid sites, as proven by the in situ ESR study. However, FTIR evacuation and ²⁷Al NMR revealed that the reduction in the amount of extraframework Al (EFAl) is due to its interaction with the nitrate group on the outside of the catalyst surface. The N/HSi@BEA catalyst exhibited high acidic strength because of the existence of more Si(OH)Al, which was initiated during the nitrate-incorporation process. Of significance is that the catalytic performance of *n*-hexane isomerization in the presence of hydrogen reached 50.3% product isomer yield at 250 °C, which might be ascribed to the presence of P–OH active sites that are responsible for accepting electrons, forming active protonic acid sites. NO₃–EFAl interaction induced the formation of Brønsted acid sites, and higher mesopore volume favors the production of cyclohexane isomers up to 48.4% at 250 °C. This fundamental study exhibits that significant interactions given by such phosphate and nitrate groups with the unique silica fibrous BEA support could enhance isomerization, which contributes to the high quality of fuel.



1. INTRODUCTION

Currently, worldwide energy utilization increases every year, especially for transportation, which causes environment pollution and incredible energy pressure due to a lot of formation of unwanted emissions.^{1,2} Hydroisomerization has captured extensive consideration in producing a high quality fuel that can reduce pollution.^{3,4} Therefore, in order to produce green fuel, an effective strategy such as increasing the lifetime of catalysts and the yield of isomer products can improve hydroisomerization performance.^{5,6} Bifunctional catalysts that have metal sites and acid sites were operative catalysts for the hydroisomerization of *n*-alkane.⁷ During the reaction, noble metals usually provide metal sites to alkane and its alkene intermediates for promptly undergoing a process of equilibrium between dehydrogenation and hydrogenation. Subsequently, the intermediate of alkenes experiences a protonation on Brønsted acid sites of acid supports before undergoing the carbenium ion mechanism to produce isomer and crack products.⁸ Therefore, isomer product yield can be enhanced by good equilibrium among the functions of acid sites and metals, which is one of the significant factors needed to raise the catalytic performance in isomerization. To date, the introduction of alteration metal and metal load varying have

been explored by a lot of researchers in order to study in detail the effects of metal sites toward hydroisomerization.^{9,10}

Physical and chemical properties such as strong acidity, high surface area, shape selectivity, and high performance provided by microporous zeolite catalysts are extensively used in the chemical and petrochemical industries.^{4,11,12} These properties of zeolites strongly rely upon the amount of aluminum present in the zeolite framework. Thus, dealumination that occurred from the framework of the catalyst had a significant effect on the acidity and catalytic performance of zeolites. So, there are burgeoning studies discussed about the dealumination of zeolite.^{13–16} Generally, extraction of aluminum from the different types of zeolite frameworks such as mordenite (MOR), beta (BEA), and ZSM-5 (MFI) could give different behaviors of zeolites.^{17–19} Beta zeolite has a high degree of dealumination followed by mordenite and ZSM-5 for the same number of T-sites in four rings.²⁰ Aluminum in the structure of beta zeolite is easier to remove due to its higher flexibility

Received: October 2, 2019

compared to mordenite and ZSM-5. There are a lot of factors that influence the dealumination behavior of zeolite such as the silicon aluminum ratio, the zeolite structure, the size of the crystal, the amount of Brønsted acidic or defect sites, and also the method used for abstraction of Al from the catalyst structure. Earlier studies revealed that acidic properties and catalytic activity of catalysts were pretentious by dealumination of the tetrahedral Al framework via acid treatment. For that reason, the dealumination of zeolite has to be a focus of most work.^{17,18,21}

In the past two decades, phosphorus has been one of the promoters of interest to improve hydrothermal stability, especially for ZSM-5.^{22–24} Furthermore, phosphorus gave positive influences on catalyst acidity, especially on the Brønsted acidity of the catalyst.^{25,26} Initial research by Mobil stated that phosphorus in oxide form was incorporated in zeolite pores analyzed from their prepared alteration of zeolites.²⁶ Incorporation of phosphorus with Y,^{27,28} and especially ZSM-5,^{23,24,29} has been studied by numerous researchers. Acidic properties of zeolite Y were changed due to the formation of different surface aluminophosphates after the addition of phosphorus in the form of H₃PO₄.²⁸ In zeolite ZSM-5,^{22,24,29,30} the phosphorus compounds are preferred to interact with bridge hydroxyl groups, leading to affecting the catalytic activity and modifying shape selectivity due to the decrease in zeolite acidity. Caro et al.³¹ described the reduction of acidic properties of the catalyst by the formation of aluminum phosphate upon framework dealumination; however, Seo et al.³² observed no removal of the Al framework after introduction of phosphorus, and they ascribed the interaction of the catalyst with phosphorus to a reduction of Brønsted acidity due to the formation of octahedral aluminum. Lischke et al.³³ revealed that hydrothermal treatment of the phosphate group loaded on ZSM-5 by impregnation preserves the high Brønsted acid site. However, Blasco et al.²⁹ found that bridge OH located in the ZSM-5 channels preferred to react with H₃PO₄ and NH₄H₂PO₄. They also observed that the properties of phosphorus incorporated in the ZSM-5 catalyst showed no significant changes when using different sources of phosphorus treatment. In addition, nitric acid treatment over BEA zeolite was studied by Baran et al., who demonstrated the dealumination occurred at a faster rate when BEA was treated up to 0.08 h. The concentration of Lewis and Brønsted acid sites present in the dealuminated BEA zeolite was influenced by the technique used to remove Al atoms and the amount of Al atoms dislodged from the catalyst structure.¹⁴ However, it seems that the details of the interaction between nitrate and phosphate with BEA zeolite and the nature of the acid sites in the hydroisomerization of cyclic and noncyclic hydrocarbon are worthy of further clarification.

In this work, we attempt to introduce phosphate and nitrate groups on highly accessible-active-site catalysts, bicontinuous silica lamellar HBEA, for comparison of *n*-hexane and cyclohexane hydroisomerization activity. For this purpose, we provide a better understanding of the physicochemical processes that take place during impregnation of phosphoric or nitric acid over the bicontinuous silica lamellar HBEA catalyst (HSi@BEA), and we obtain qualitative insights into phosphate–catalyst or nitrate–catalyst interactions that give different routes during *n*-hexane and cyclohexane hydroisomerization. A new plausible structure mechanism was proposed in accordance with catalyst characterization and the catalyst activity test.

2. EXPERIMENTAL SECTION

2.1. Catalyst Preparation. A modified microwave supported by the hydrothermal treatment technique was used to synthesize the fibrous silica beta.^{34,35} Toluene (28 mol) and 1-butanol (1.62 mol) were mixed before the addition of 1 mol of tetraethyl orthosilicate in the mixture. A solution of urea (0.9 mol) and cetyltrimethylammonium bromide (0.27 mol) was dissolved in distilled water by string for 15 min at ambient temperature. Subsequently, the BEA seed was then added and magnetically stirred for 30 min. The resultant solution was irradiated with 400 W microwave radiation at 120 °C intermittently for 6 h. The catalyst was centrifuged, washed with acetone and distilled water, and then dried in an oven at 100 °C overnight. The dried solid was then calcined using a furnace at 550 °C for 6 h. The sample was labeled as the Si@BEA catalyst. Then, ammonium nitrate(V) solution was used in two cycles of the protonation process of the Si@BEA catalyst before being dried at 120 °C overnight and calcined at 550 °C for 3 h to give HSi@BEA.

The phosphate and nitrogen ion treated HSi@BEAs were synthesized via impregnation of the HSi@BEA with 0.5 N H₃PO₄ (aq) and HNO₃ (aq) solution, respectively, followed by drying at 120 °C overnight and calcination at 550 °C in air. The catalysts were then denoted as P/HSi@BEA and N/HSi@BEA, respectively.

2.2. Catalyst Characterization and Reaction Study. The catalysts' diffraction plots were collected on a Bruker Advance D8 X-ray powder diffractometer (Cu K α radiation source, 40 mA, 40 kV) in the range of $2\theta = 5\text{--}70^\circ$ to confirm the crystallinity of catalysts. Field emission scanning electron microscopy (JSM-6710 F) and transmission electron microscopy (Philips EM420) were used to examine the surface morphology of catalyst. Catalysts were subjected to an outgassing step at 300 °C for 1 h and then underwent N₂ adsorption at -196°C via Beckman Coulter SA 3100. Fourier transform infrared (FTIR) analyses were performed with an Agilent Carry 640 FTIR Spectrometer. FTIR with the KBr method was used to analyze chemical functional groups of samples within a scan rate of 400–4000 cm⁻¹. Concisely, acidity measurement was performed in an in situ process using a basic probe molecule, 2,6-lutidine. The catalyst was evacuated at 400 °C for 1 h. Then, the evacuated samples experienced adsorption with 4 Torr of 2,6-lutidine (15 min) before desorption at 50–200 °C. A Bruker Advance 400 MHz 9.4 T spectrometer was used to perform ²⁷Al MAS NMR by means of a spin rate of 7 kHz, a pulse length of 1.9 μs , and a relaxation time delay of 2 s. The formation of unpaired electrons was evaluated by a JEOL JES-FA100 ESR spectrometer. The catalysts were introduced with hydrogen gas (100 Torr) at RT after being outgassed at 400 °C for 1 h.

A microcatalytic pulse reactor was used to perform isomerization of *n*-hexane under atmospheric pressure at 423–523 K. The gas feed (hydrogen) flow was 100 mL/min. A total of 0.2 g of the catalyst underwent activation at 400 °C (3 h) and then cooled to the favored reaction temperature. Once 1 μL of *n*-hexane was injected, the liquid product was kept at -196°C , and the products were detected using a 6090N Agilent GC FID detector equipped with an HP-5 capillary column. Then, the process was repeated using cyclohexane as a feed. Equation 1 and eq 2 were used to consider the isomers' selectivity (S_i) and yield (Y_i).

$$S_i = \frac{C_i}{\sum C_i - C_{\text{res_reactant}}} \times 100\% \quad (1)$$

$$X_{\text{reactant}} = \frac{\sum C_i - C_{\text{res_reactant}}}{\sum C_i} \times 100 \quad (2)$$

$$Y_i = \frac{X_{\text{reactant}} \times S_i}{100} \quad (3)$$

where C_i is the isomer mole fraction in the stream of the product and $C_{\text{res_reactant}}$ is the residual reactant.

3. RESULTS AND DISCUSSION

3.1. Crystallinity and Morphological and Textural Studies. Figure 1A shows the XRD patterns of HSi@BEA, P/

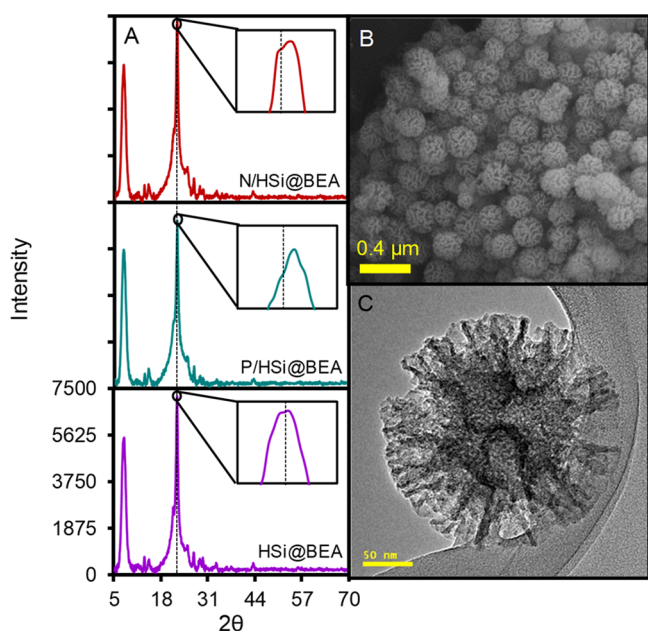


Figure 1. (A) XRD patterns of HSi@BEA, P/HSi@BEA, and N/HSi@BEA. (B) FESEM and (C) TEM images of HSi@BEA.

HSi@BEA, and N/HSi@BEA catalysts. The diffraction peaks of all catalysts appeared at $2\theta = 7.8^\circ$, 22.47° , 27.1° , 29.6° , and 43.6° , which are similar to the usual diffraction patterns of the BEA zeolite (JCPDS No. 48-0074).³⁶ The peak at $2\theta = 22.47^\circ$ is magnified in the inset figures to show the differences in intensity and probable shift of the peak in the catalysts. It was observed that the loading of phosphate and nitrate into the HSi@BEA support decreased the peak intensity by 0.6% and 0.4%, respectively. The shift in the corresponding peak specified the dealumination of the catalyst framework.^{37–39} Shifting of $2\theta = 22.46^\circ$ for the parent beta to $2\theta = 22.50^\circ$ for hydrochloric acid treatment, followed by steaming of the beta catalyst, was claimed due to dealumination of the catalyst framework, as conveyed by Wang et al.³⁷ The disturbance of the parent framework was most probably due to the acid treatment during the impregnation of phosphate and nitrate groups on the catalyst, which could affect the extra-framework aluminum species (EFAl).^{14,17,40} Zhao et al. revealed that after modification of HZSM-5 with phosphoric acid, the structure and acidity of the catalyst were affected due to the extraction of tetrahedral aluminum in the catalyst framework to the extra-framework.⁴¹

FESEM and TEM were used to analyze the morphological properties of the HSi@BEA catalyst, as demonstrated in Figure 1B and C, respectively. It was clearly observed that the HSi@BEA catalyst contained typical microspheres, with a bicontinuous concentric lamellar morphology. Similarly, an identical morphology was observed despite the addition of phosphate and nitrate groups by the impregnation method (Figure S1). These correlated with the XRD results, which showed the preservation in crystallinity of the catalysts after the introduction of phosphate and nitrate groups. Elemental mapping showed that the silica amount was more highly dispersed than that of Al, which was most likely because of the

silicon aluminum ratio of the parent HSi@BEA catalyst used (32).⁴² Furthermore, P atoms have a higher distribution compared to N atoms. This might be associated with the lower electronegativity of P associated with N atoms, which can react with hydroxyl groups of the catalyst framework. Meanwhile, the TEM image of HSi@BEA (Figure 1C) illustrates the dendrimeric fibrous structure covering the catalyst core, which could contribute to the high surface area, besides giving more active sites for subsequent reactions.

Figure 2A demonstrates the UV-DRS spectra of all catalysts in the area of 200–400 nm. Peaks at 223, 245, 300, and 340

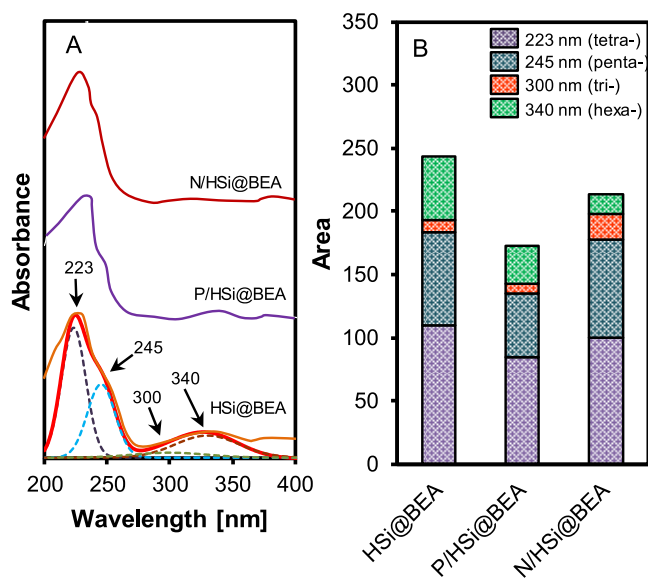


Figure 2. (A) UV-DRS spectra for all catalysts. (B) Gaussian peak area of deconvoluted peaks shown in Figure 2A.

nm, in the Gaussian fitting, reveal the presence of tetra-, tri-, and hexa-coordinated elements in the HSi@BEA, P/HSi@BEA, and N/HSi@BEA catalysts.^{43–46} For a better view, the Gaussian peak area of the above-mentioned peaks is summarized in Figure 2B. Generally, in comparison with the parent HSi@BEA catalyst, P/HSi@BEA shows the lowest area of all corresponding peaks, demonstrating the greatest disturbance of the catalyst framework. The N/HSi@BEA catalyst exhibits a higher peak area of tri- and penta-coordination compared to parent HSi@BEA and P/HSi@BEA catalysts, which could be due to more dealumination occurring with respect to the additional formation of EFAl species.^{47,48} The decrease in hexa-coordination in the N/HSi@BEA catalyst as compared to the parent HSi@BEA suggested an interaction between the nitrate group and both frameworks.

Figure 3 illustrates the N_2 physisorption isotherms and NLDFT analysis of the catalysts. As can be seen, all catalysts exhibited a characteristic isotherm of microporous materials at a lower P/P_0 , while mesoporous materials of type IV with an H1 hysteresis loop contain intraparticle and interparticle pores.^{4,49} The textural properties of the catalysts were possibly changed after the addition of phosphate and nitrate groups, which was indicated by the change in the isotherm of the catalysts. The BET specific surface areas for HSi@BEA, P/HSi@BEA, and N/HSi@BEA catalysts were 619, 361, and 486 $m^2 g^{-1}$, respectively (Table 1). After the addition of phosphate and nitrate groups, the decrease in surface area confirmed the successful loading of both species on the HSi@BEA catalyst.⁵⁰

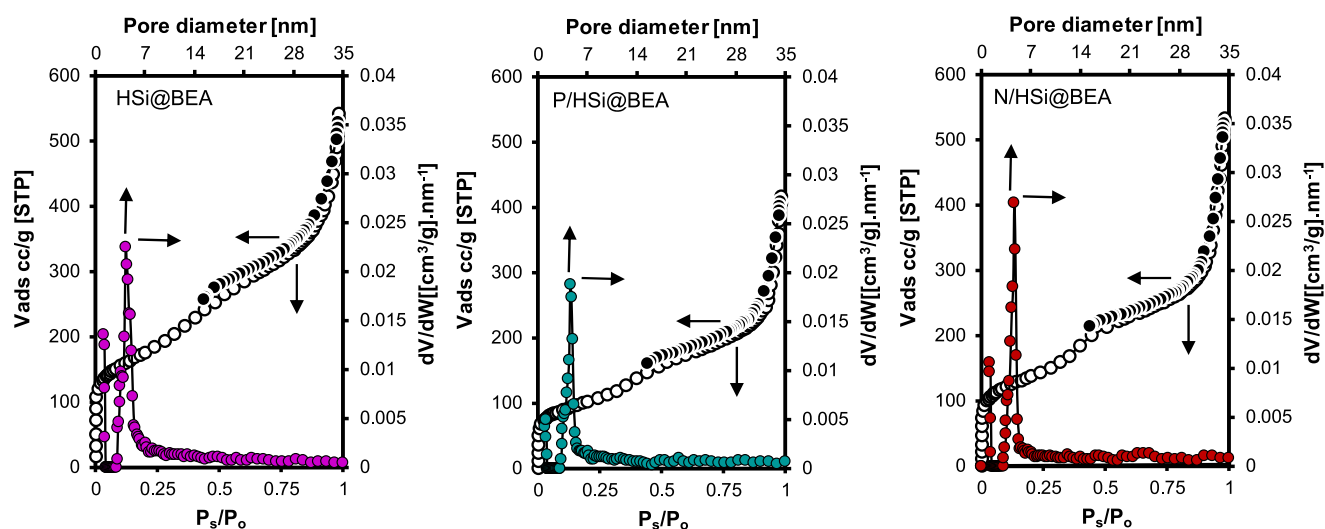


Figure 3. N₂ adsorption (white-circle symbol)—desorption (black-circle symbol) isotherms and NLDFT pore size distribution (colored-circle symbol) of HSi@BEA, P/HSi@BEA, and N/HSi@BEA catalysts.

Table 1. Physicochemical Properties of All Catalysts and Presence of Hydrogen

catalysts	BET surface area (m ² g ⁻¹)	micropore volume (cm ³ g ⁻¹)	mesopore volume (cm ³ g ⁻¹)	average pore (nm) ^a	ν _{TOT} (cm ⁻¹)	Weize–Prater value (10 ⁻⁶)		activation energy (kJ mol ⁻¹)	
						<i>n</i> -hexane	cyclohexane	<i>n</i> -hexane	cyclohexane
HSi@BEA	619	0.0647	0.748	5.75	1084	1.08	1.51	21.6	15.8
N/HSi@BEA	486	0.0521	0.774	6.52	1090	5.20	4.18	16.9	10.6
P/HSi@BEA	361	0.0305	0.592	6.35	1086	3.22	4.38	8.65	10.7

^aAverage pore was calculated was calculated from NLDFT.

The N/HSi@BEA catalyst displayed a rise in mesopore volume; this could be due to the dealumination, which is in agreement with UV-DRS results. The obvious decrease in micropore and mesopore volumes, as well as surface area of the P/HSi@BEA catalyst, is most likely correlated with the same phenomenon as above, but with replacement of Al with the larger P atoms.^{51–53}

The ²⁷Al MAS NMR spectra of HSi@BEA, P/HSi@BEA, and N/HSi@BEA catalysts in high (A,B,C) and low (D,E,F) ranges, respectively, are shown in Figure 4. According to the deconvoluted peaks of the parent HSi@BEA catalyst (Figure 4A), there are four peaks belonging to a tetrahedral coordination of the aluminum which are located at 60, 55, 50.5, and 46 ppm.^{13,54} The first peak is associated with the tetrahedrally coordinated extra-framework Al. However, the peak at 46 ppm is attributed to penta-coordinated Al species or distorted tetrahedral Al in the framework or extra-framework. After impregnation with phosphoric acid (Figure 4B), the peaks at 55 and 50.5 ppm decreased markedly and shifted to 54.5 and 49.6 ppm due to dealumination of the catalyst framework. In addition, the peak intensity of the shifted peaks decreased markedly with the concomitant increased peak intensity at 43.2 ppm, suggesting that the phosphate group interacts with Si–O–Al in the catalyst framework. This is in agreement with the result of the BET and UV-DRS. Liu et al. reported similar results, in which dealumination resulted in a drop in peak intensity of tetrahedral Al and the appearance of distorted tetrahedral Al peaks.²³ However, different results were reported by Lischke et al., which claimed that the degree of dislodgement of some aluminum atoms from the framework

of phosphate-impregnated HZSM-5 was lower than that of nonimpregnated catalysts, demonstrating that Al ions at substitutional positions in the SiO₂ framework were partially protected by phosphorus from being removed from its original position.³³ The catalyst impregnated with nitric acid gave similar results, decreasing and shifting the tetrahedrally coordinated Al of the N/HSi@BEA catalyst because of the detachment of Al from the catalyst framework (Figure 4C). Nevertheless, the peak intensity at 54.3 ppm obviously decreased with a simultaneous increase in the peak at 49.6 ppm, attributed to the transition from the tetrahedrally coordinated Al to either penta-coordinated Al or distorted tetrahedral Al.³⁹

In addition, the octahedrally coordinated framework and extra-framework Al for the parent HSi@BEA catalyst were manifested at 0 and –1.5 ppm, respectively, as displayed in Figure 4D. The peak at –1.5 was shifted to –1.8 ppm after the incorporation of phosphate and nitrate groups, indicating the preferable Al atoms' exclusion from the structure (Figure 4E and F). This clarification is consistent with previous studies which exhibited preferential removal of Al atoms placed in particular tetrahedral sites of the acid leaching MOR zeolites.^{4,21} However, a new peak appeared at –5.8 ppm for the N/HSi@BEA catalyst, which is attributed to the distorted octahedral Al species.³⁷ This was probably due to the interaction of the nitrate group with some extra-framework Al. Thus, we can summarize that the amount of EFAl species present in all catalysts is in the following order: HSi@BEA > N/HSi@BEA > P/HSi@BEA.

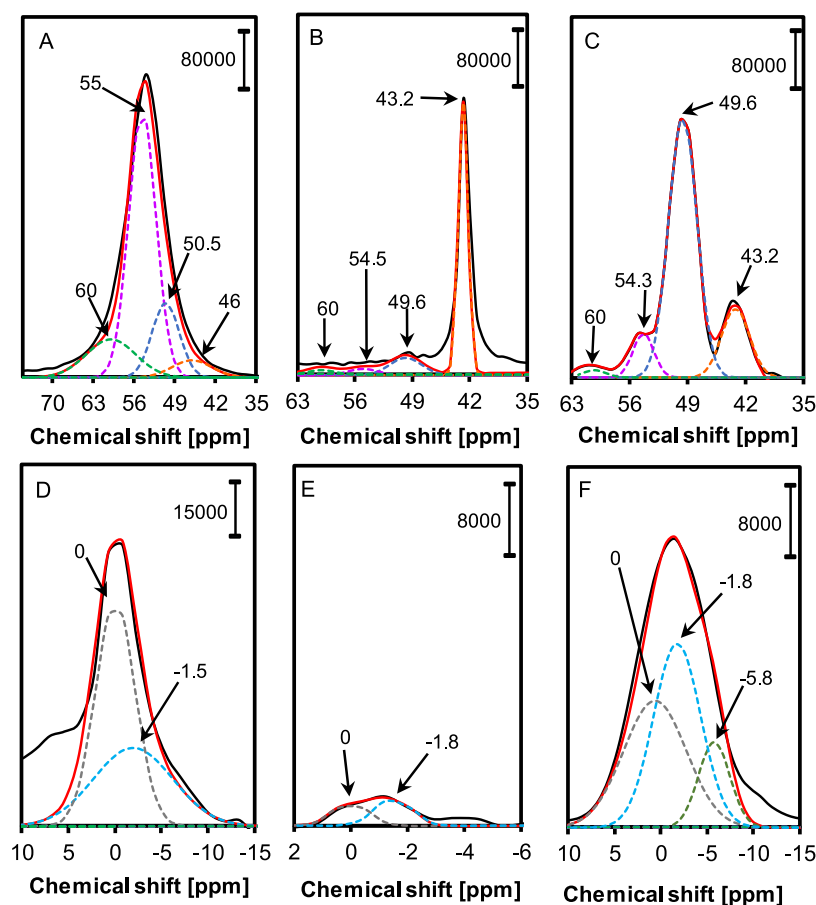


Figure 4. ^{27}Al -NMR spectra for HSi@BEA, P/HSi@BEA, and N/HSi@BEA catalysts at high and low ranges.

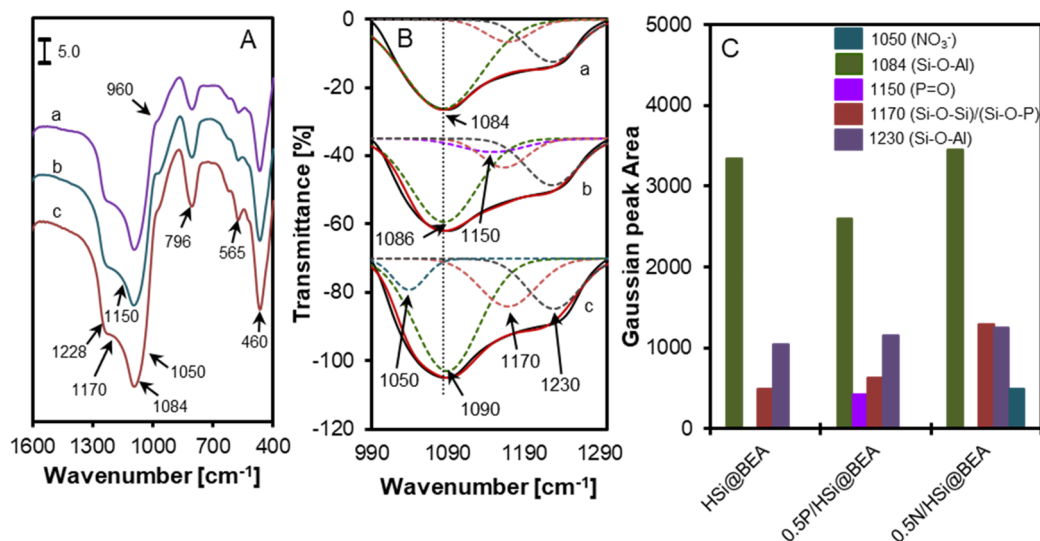


Figure 5. FTIR spectra of (a) HSi@BEA, (b) P/HSi@BEA, (c) N/HSi@BEA. (B) Deconvolution range of 990–1300 cm^{-1} and (C) Gaussian peak area of the deconvoluted peaks.

3.2. Vibrational Spectroscopy. FTIR spectra show the internal and external bending and stretching vibrations found in zeolites, which are depicted in Figure 5A. All catalysts exhibited characteristic bands identified at 1230, 1170, 1150, 1084, 1050, 960, 796, 565, and 460 cm^{-1} . Deconvolution peaks of the FTIR pattern in the 1300–990 cm^{-1} range are shown in Figure 5B. External and internal asymmetric stretching and symmetric stretching appeared at bands 1230, 1084, and 796

cm^{-1} , respectively, while the band at 460 cm^{-1} was because of the bending mode vibration of T–O–T in the framework and corresponds to Si–O–Al materials.^{55,56} Meanwhile, the external silanol groups (Si–O–H) produce a characteristic band at 960 cm^{-1} . There are two bands centered at 565 and 525 cm^{-1} , which are representative of five- and six-membered rings of T–O–T (T = Si or Al) vibrations of beta zeolite, implying that beta zeolite is preserved in the samples.⁵⁵ The

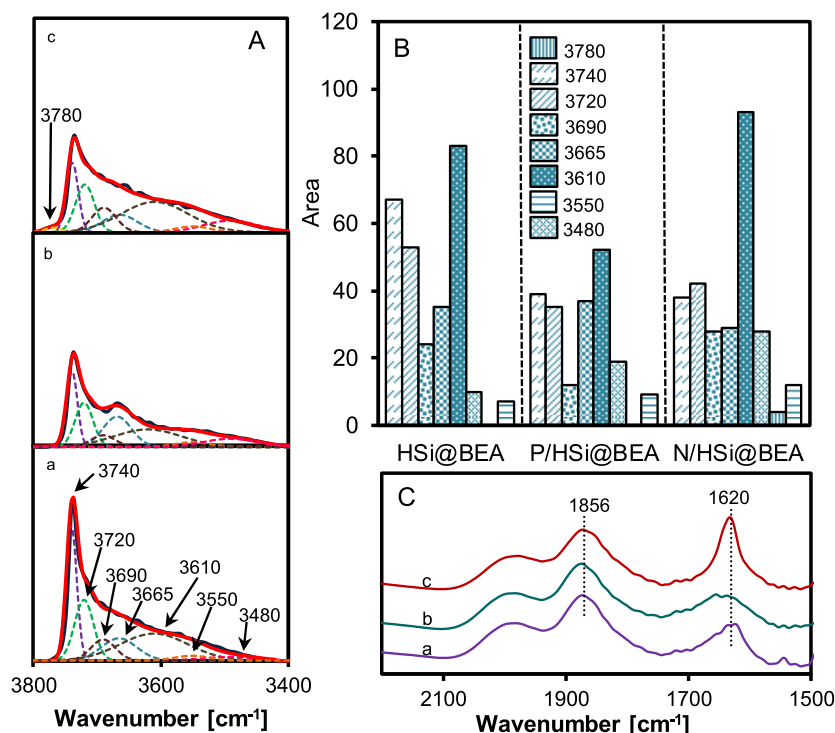


Figure 6. FTIR spectra for (a) HSi@BEA, (b) P/HSi@BEA, and (c) N/HSi@BEA in the range of (A) 3800–3400 cm^{-1} . (B) Gaussian peak area of evacuated peaks and (C) 2200–1500 cm^{-1} .

appearance of bands at 1150 and 1050 cm^{-1} relate to $\text{P}=\text{O}$ and NO_3^- , respectively, signifying the probable contribution of those species on the HSi@BEA support.^{57–59} The band at 1170 cm^{-1} was ascribed to asymmetrical stretching vibrations of Si–O–Si or Si–O–P bonds. To determine the desilication and/or dealumination of the zeolite framework for determining the accurate the catalysts' structure, the Gaussian peak areas of the above-mentioned bands (1230, 1170, 1150, 1084, and 1050 cm^{-1}) are summarized in Figure 5C. The asymmetrical stretching vibration of the T–O–T framework at 1084 cm^{-1} for the parent catalyst (HSi@BEA) shifted to 1090 cm^{-1} for the N/HSi@BEA catalyst, suggesting framework dealumination.^{37,60} The P/HSi@BEA catalyst showed a slight shift in the ν_{TOT} value (1086 cm^{-1}) from the parent catalyst, which indicates that some aluminum atoms are hard to remove due to high stability, and only a few Al atoms were removed to give EFAL.³⁷

Deconvolution of the FTIR spectrum of HSi@BEA, P/HSi@BEA, and N/HSi@BEA catalysts in the 3800–3400 cm^{-1} range by Gaussian curve-fitting (Figure 6A) showed that the spectrum consisted of eight bands at 3780, 3740, 3720, 3690, 3665, 3610, 3550, and 3480 cm^{-1} . For a better view, the deconvoluted peak areas are presented in Figure 6B. Two major bands were observed at 3740 (isolated terminal silanol group (Si–OH)) and 3610 cm^{-1} (bridging hydroxyl groups [Si(OH)Al]).^{42,46} Furthermore, the 3780 and 3665 cm^{-1} bands are related to the atoms of the tricoordinated aluminum that partly connected to the framework and extra-structure aluminum types, respectively, while the peaks at 3720 and 3690 cm^{-1} correspond to the oxygen in the silanol group that interacts with a side electron pair acceptor site.^{41,42,46,55} Moreover, the weak broad bands that appeared at 3550 and 3480 cm^{-1} are attributed to connecting hydroxyls agitated by H-bond interaction with the zeolitic framework and hydroxyl

nests, respectively. The latter band is attributed to Si–OH defect bonds hydrogen bonded to the oxygen in the framework.⁶¹ From the summary of the deconvoluted band areas shown in Figure 6B, it is obvious that areas of the bands changed significantly, indicating that those species interacted with both acidic and nonacidic hydroxyl groups after the introduction of phosphate and nitrate groups.⁴² Notably, the perturbation of external OH groups for the formation of Si–O–P and/or new Si–O–Si bonds, as well as dealumination, diminished the amount of terminal silanol groups (3740 cm^{-1}), which were also caused by the presence of phosphate and nitrate groups.⁶² In addition, a broad shoulder band attributed to silanol nests (3480 cm^{-1}), resulting from dealumination and/or desilication, was also increased after impregnation of phosphoric and nitric acid.^{61,63,64} However, the larger increase in the 3480 cm^{-1} band after incorporation of nitrate compared to that of the phosphate group is most likely due to the higher tendency for the dealumination and/or desilication process to occur.^{14,18} From Figure 6A,B, it could be observed that the Brønsted acid sites greatly decreased after incorporation of phosphate groups, indicating a weakening in acid sites by the existence of that species.^{15,53} In previous studies, it was reported that the acid site numbers increased significantly after impregnation of H_3PO_4 on the catalyst and that they are much weaker than unmodified catalysts in terms of strength.^{25,31,65,66} Some studies have claimed that the dealumination, which was tempted by thermal and acid treatment, caused the loss of Brønsted acid sites.²³ The higher appearance of EFAL species at 3665 cm^{-1} in P/HSi@BEA compared to the N/HSi@BEA catalyst was evident from the results in Figure 6A,B, indicating that the phosphate group did not interact with EFAL. The results also suggested that the nitrate group was probably bonded with EFAL species at the external surface of the catalyst. After introduction of the nitrate

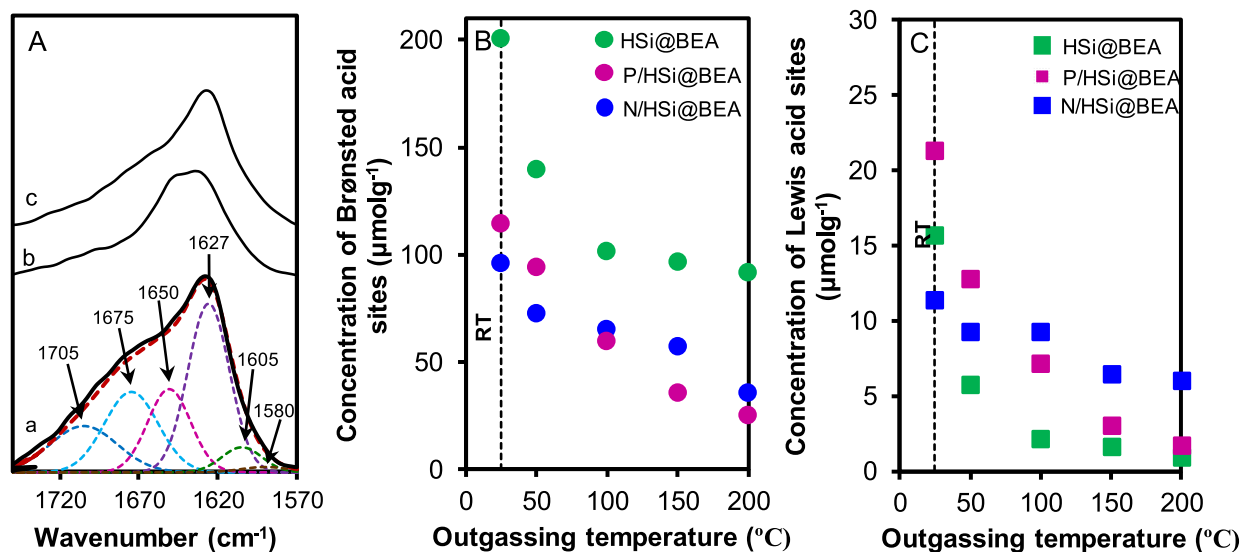


Figure 7. (A) IR spectra of 2,6-lutidine adsorbed on (a) HSi@BEA, (b) P/HSi@BEA, and (c) N/HSi@BEA at room temperature. Variations of concentration of (B) Brønsted and (C) Lewis acid sites for all the catalysts as a function of outgassing temperature from 50 to 200 °C after 2,6-lutidine adsorption.

group (Figure 6A,C), the reduction in the peak at 3665 cm^{-1} and the growth of the 3610 cm^{-1} peak specified the formation of EFAl-NO₃ via the NO₃⁻ coordinatively interacted with acidic hydroxyl groups corresponding to extra-framework aluminum.⁶⁷

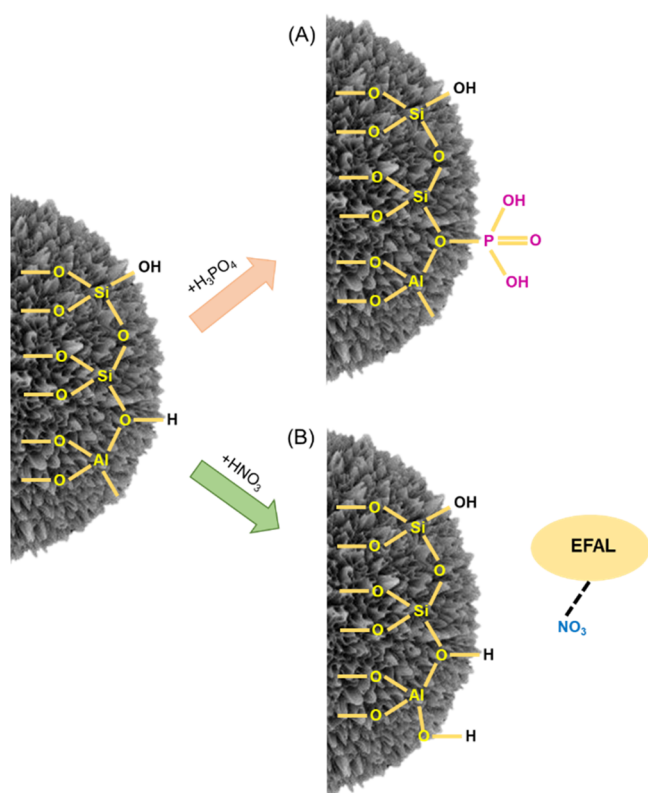
Figure 6C displayed the catalysts' stretching frequency of the vibrational lattice in the range of $2200\text{--}1500\text{ cm}^{-1}$. All catalysts exhibited bands at 1856 and 1620 cm^{-1} , which corresponded to the association of Si atoms with four other -O-Si- atoms, and the latter band relates to the Si-O-Si or Si-O-H bonding.⁶⁸ No significant change in the former band was observed for N/HSi@BEA, with a marked increase in the latter band compared to the P/HSi@BEA catalyst. These results were due to the formation of more Si-O-H (1620 cm^{-1}) in N/HSi@BEA than that of the P/HSi@BEA catalyst as a consequence of dealumination of the catalyst framework.

3.3. Acidity Studies. Deconvolution of the bands shown in Figure 7A by Gaussian curve fitting was caused in six major absorption bands at 1705 , 1675 , 1650 , 1627 , 1605 , and 1580 cm^{-1} . The lutidinium cation was coordinately bonded to the protonic sites linked to the formation of bands at 1705 , 1675 , 1650 , and 1627 cm^{-1} , although the bands at 1605 and 1580 cm^{-1} appeared due to the unbrokenness of lutidine with Lewis acid sites.⁵⁵ The strengths of the Brønsted and Lewis acid sites as an outgassing temperature function for HSi@BEA, P/HSi@BEA, and N/HSi@BEA are demonstrated in Figure 7B and C. The spectra of all catalysts are shown in Figure S3. The results show important changes above 150 °C because the isomerizations of *n*-hexane and cyclohexane were active above 150 °C . It is observable that the parent HSi@BEA catalyst possesses the highest Brønsted acid sites, followed by N/HSi@BEA and P/HSi@BEA catalysts. However, the HSi@BEA catalyst had the weakest Lewis acid site nature, with acidic strength enhanced by the addition of nitrate and phosphate groups. The presence of phosphate in the catalyst framework caused weaker Brønsted and Lewis acid sites compared to the nitrate-loaded catalyst. This was verified by the higher desorption of the lutidinium ion from the P/HSi@BEA catalyst above 100 °C of the elevated temperature. The phosphatation affects the weak acid site less than the strong

acid sites because of the amount of escalation of the latter acid sites after modification.⁶⁷ This was conspicuously ascribed to development of the P-OH groups that are presented in the framework-incorporated phosphate groups. The lutidinium ion is strongly attached on the N/HSi@BEA catalyst, which shows a slight reduction in the concentration of both Brønsted and Lewis acid sites throughout the outgassing temperature. This can be dictated that the loading of nitrate groups, which affords an essential concentration increase of strongly acidic Si(OH)Al groups (3610 cm^{-1}), in agreement with the FTIR evacuation results.

3.4. Proposed Structure of P/HSi@BEA and N/HSi@BEA. According to the considered and experimental results, a model of the phosphate group or nitrate group incorporated into the HSi@BEA catalyst is proposed in Scheme 1. Extra-framework Al species (Al³⁺, AlO⁺, Al(OH)₂⁺, or Al(OH)₂²⁺, or Al_xO_yⁿ⁺) also act as Lewis acid sites in the catalysts.^{4,13} It is proposed that the inclusion of a phosphate group in HSi@BEA was formed by replacing OH⁻ with a H₂PO₄⁻ group via hydrolysis during the calcination process. The Brønsted acid sites' strength was significantly affected by the replacement of the Brønsted acidic hydroxyl group with a H₂PO₄⁻ group. The existence of P-OH reduced the Brønsted acid sites' strength due to the terminal position of its hydroxyl group, which has a lower acidic strength than the bridging hydroxyl.^{67,69} Furthermore, this also resulted in an increase in the acid sites number. After introduction of a nitrate group, some framework Al was transformed to octahedral extra-framework Al and interacted with the nitrate ion to form EFAl-NO₃ as a result of dealumination. This led to an escalation in the strength of Brønsted acid sites, resulting from the formation of a new bridge hydroxyl group. For the catalytic mechanism, generally, hydrogen molecules undergo dissociation to hydrogen atom formation, which then diffuses to Lewis acid sites of the catalysts. Protonic acid sites were generated when the atomic hydrogen lost an electron to Lewis acid sites. The Lewis acid sites that accept the electron react with another hydrogen atom to cause a hydride formation which associated to the Lewis acid site. This phenomenon gives rise to the formation of protonic acid sites and hydride on the surface of P/HSi@

Scheme 1. Possible Structure of (A) Phosphate and (B) Nitrate on HSi@BEA



BEA and N/HSi@BEA catalysts. The model of acid sites and catalyst structure was proposed depending on the results obtained in this study and the previous report as presented in Scheme 1. The hydrogen adsorption during isomerization resulted in H^+ and H^- formation, where H^+ is placed on the O atom near the cus (coordinating unsaturated) metal cation to form OH (active sites). However, for the P/HSi@BEA catalyst, H^+ is placed on the O atom near the P atom resulting in P–OH formation, which is the active site for the catalyst. When 2,6-lutidine was adsorbed on the catalyst, 2,6-lutidine was corresponding to the cus Al. The hydrogen atom provided an electron to the cus Al and became the acidic OH after the hydrogen was adsorbed on the lutidine-precursor catalyst. The cus Al became Al^- and decreased the Lewis acidity. The 2,6-lutidine adsorbed on the cus Al is effectively desorbed and moves to the acidic OH to form a lutidinium ion. The cus Al responds with other hydrogen atoms to form cus-Al clinging to hydride. Clearly, the model suggested for the acidic center structure is theoretical. Nevertheless, the model might have the option to decipher the outcomes acquired in the present investigation and those revealed in the literature.

3.5. Catalytic Testing. The activities of HSi@BEA, P/HSi@BEA, and N/HSi@BEA catalysts were performed on *n*-hexane and cyclohexane at temperatures of 100–350 °C, and the outcomes are listed in Table 2. The results show that the percentage of *n*-hexane and cyclohexane conversion increased significantly with increasing reaction temperature. As summarized in Figure 8A and B, higher conversion of *n*-hexane was dominated by P/HSi@BEA, while the N/HSi@BEA catalyst was highly favorable for cyclohexane conversion. For *n*-hexane conversion (Figure 8A), the acid-impregnated catalyst increased nearly 4 times more than the parent catalyst

Table 2. Product Distributions of *n*-Hexane and Cyclohexane Isomerization in the Presence of Hydrogen

	reaction temperature [°C]				
	150	200	250	300	350
<i>n</i> -hexane					
HSi@BEA					
conversion (%)	5.8	12.5	19.8	27.1	22.0
selectivity of isomers (%)	100	100	80.0	75.2	48.0
selectivity of cracking products (%)	0	0	19.9	23.8	52.0
yield of isomers products	5.8	12.5	18.6	26.8	22.0
P/HSi@BEA					
conversion (%)	26.1	32.7	50.3	58.1	65.2 (53) ^a
selectivity of isomers (%)	100	100	100	70.5	57.0 (44.8) ^a
selectivity of cracking products (%)	0	0	0	29.5	43.0 (54.2) ^a
yield of isomers products	26.1	32.7	50.3	41.0	37.2 (23.7) ^a
N/HSi@BEA					
conversion (%)	20.8	24.0	27.2	47.2	51.9
selectivity of isomers (%)	100	100	100	45.5	26.0
selectivity of cracking products (%)	0	0	0	54.5	74.0
yield of isomers products	20.8	24.0	27.2	21.5	13.5
cyclohexane					
HSi@BEA					
conversion (%)	4.7	10.4	18.8	26.8	32.9
selectivity of isomers (%)	100	100	70.2	24.8	10.8
selectivity of cracking products (%)	0	0	28.8	74.2	88.2
yield of isomers products	4.7	10.4	13.2	6.65	3.55
P/HSi@BEA					
conversion (%)	21.4	29.1	43.3	54.0	39.3
selectivity of isomers (%)	100	100	85.1	63.1	15.3
selectivity of cracking products (%)	0	0	14.9	36.9	84.7
yield of isomers products	21.4	29.1	36.8	30.3	6.02
N/HSi@BEA					
conversion (%)	18.8	34.6	48.4	70.3	89.8 (62.6) ^a
selectivity of isomers (%)	100	100	100	49.8	14.6 (6.8) ^a
selectivity of cracking products (%)	0	0	0	50.2	85.4 (92.2) ^a
yield of isomers products	18.8	33.3	48.4	35.0	13.1 (4.26) ^a

^aIn the experiment conducted, 10 pulses were measured at each reaction temperature. The activity in Table 2 was taken from the average of the sixth, seventh and eighth pulses, in which the activity was stable.

(HSi@BEA) at a reaction temperature of 150 °C. The gradual increase in the conversion from P/HSi@BEA at the elevated temperature reached 65.2% due to the moderate acidity of the catalyst, which was triggered by the structure of phosphate in the framework. At 150–250 °C, the nitrate-loaded catalyst slightly converted *n*-hexane to its products and started to increase apparently at 300 °C, probably assisted by thermal behavior, to form isomers and cracking products. In contrast, the conversion of cyclohexane using the N/HSi@BEA catalyst increased markedly up to 89% at 350 °C. Nevertheless, the P/HSi@BEA catalyst gave 54% cyclohexane conversion at 300 °C and continuous falloff by 14% at high temperatures. Insignificantly, both acid-loaded catalysts demonstrated different cyclohexane conversions at reaction temperatures below

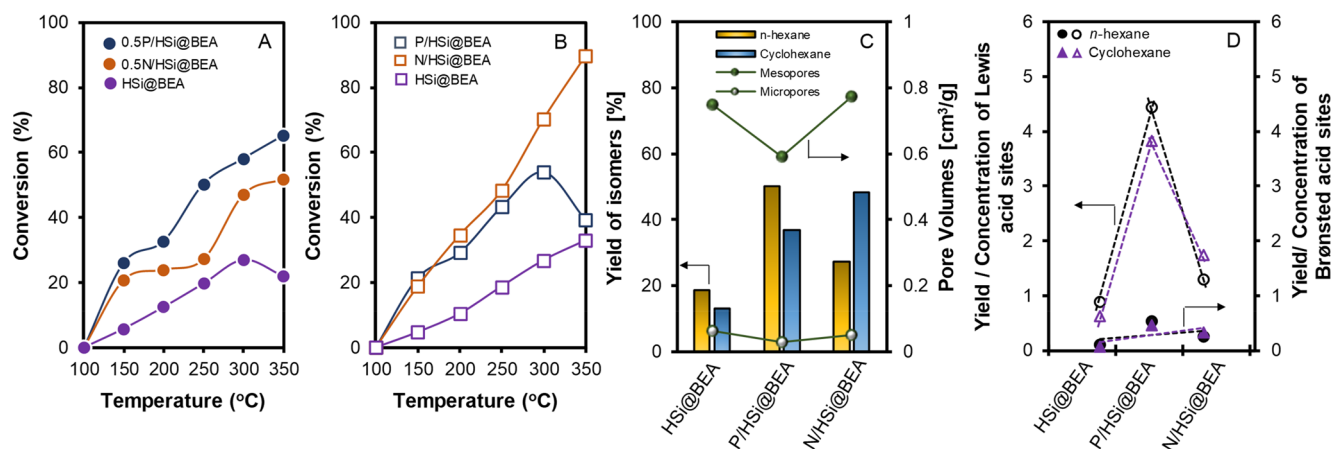


Figure 8. Percentage of conversion of (A) *n*-hexane and (B) cyclohexane as a function of temperature. (C) Relationship between yield of isomers and pore volumes of all the catalysts. (D) Dependence of the percentage yield of all the catalysts on Brønsted and Lewis acid sites

250 °C. The properties displayed in Figure 8C and D could justify these consequences. Figure 8C shows the relationship between the yield of isomers and the mesopore volume for each catalyst. From this figure, it is clear to see that the yield of isomers seems linearly related with the pore volumes. The highest mesopore volume possessed by the N/HSi@BEA catalyst led to a maximum in bulkier alkane production such as that of cyclohexane. This is due to the fact that the cyclohexane molecules were comparable with the pore diameters of the N/HSi@BEA catalyst, with a diameter of 6.5 nm, making it appropriate for the molecules to pass through the catalyst.⁷⁰ This result was parallel with the pore size distribution from the N₂ physisorption results. It is also clearly observed that the isomer yield from both reactants was not dependent on the micropores of P/HSi@BEA or N/HSi@BEA catalysts. For the N/HSi@BEA catalyst, the mesoporosity volume had significant roles in the production of cyclohexane isomers. Figure 8D shows the plot of the dependence of yield of isomers of all the catalysts upon acid site concentration after adsorption of 2,6-lutidine. There was no significant change in the yield ratio to Brønsted acid site concentration, which could be attributed to the clear correlation between the concentration of Brønsted acid sites and the production of isomers. The Lewis acid site showed a significant contribution to the yield of *n*-hexane and cyclohexane isomers as evidenced over P/HSi@BEA. This is in agreement with our previous statement that claimed that Lewis acid sites play an essential part in *n*-hexane and cyclohexane isomerization.⁴² However, the P/HSi@BEA catalyst exhibited a significantly higher contribution of Lewis acid sites for the production of *n*-hexane isomers compared to the N/HSi@BEA catalyst.

The formation of isomers in *n*-hexane isomerization remarkably upsurged when using the P/HSi@BEA catalyst as compared to N/HSi@BEA, with a maximum yield (2,3-dimethylbutane, 2-methylpentane, and 3-methylpentane) of approximately 50% at 250 °C. The isomer selectivity for the particular catalyst was decreased to 57% at 350 °C, suggesting the formation of cracking products, which was affected by the hydrothermal conditions. The cracking products took place in parallel with isomerization at high temperatures, which might also lead to deposition of coke on the catalyst. The N/HSi@BEA catalyst contributed only 27% of the maximum isomer yield at 250 °C, near the maximum yield of isomers of the parent HSi@BEA catalyst (26%). This result may be due to

the production of more cracking products, which favor the high acidity of the catalyst. Thus, 2,3-dimethylbutane, 2-methylpentane, and 3-methylpentane, which are the isomers of *n*-hexane, are preferable for production from a catalyst with moderate acidity and high Lewis acid sites. Notably, the tetrahedral form of the phosphate ion that was attached to the framework reduced the acidity of the HSi@BEA catalyst, which was evident in the FTIR results.

In addition, the yield of branched isomers was approximately 3 times that (250 °C) over the nitrate ion incorporation catalyst than the parent HSi@BEA, while the branched isomer selectivity was 100% at 150 °C, which was then reduced to ~14% at higher temperatures (350 °C). When compared to the P/HSi@BEA catalyst, an abundant production of branched isomers was identified at higher temperatures compared to the production of isomers using the N/HSi@BEA catalyst. It is noted that the performance of the N/HSi@BEA catalyst was comparable to its acidity. A one-third increase in the concentration of the acid sites (Lewis acid sites) conspicuously resulted in the desired increase in activity and selectivity. The cyclohexane molecules were contented to generate isomers on N/HSi@BEA, which has a high acid strength (Figure 7) in order to assist the reactant for skeleton rearrangement.^{71,72} Isomerization of *n*-hexane was prompted by the *n*-hexane and protonic acid site interaction to result in *n*-hexyl carbenium ion formation. After that, branched hexyl carbenium ions interact with hydride ions to form *iso*-hexane and subsequently desorb from the catalyst surface. Concurrently, *n*-hexyl or *iso*-hexyl carbenium ions undergo β -scission to form cracking products. It is important to emphasize that the existence of protonic acid sites and hydride ions increases the isomerization activity. However, the cracking and β -scission of *n*-hexyl and *iso*-hexyl carbenium ion was triggered by an excessive quantity of hydride ions and protonic acid sites that led to suppression of the isomers' selectivity.

The Arrhenius equation allows us to calculate apparent activation energies (E_a) for all the catalysts over the range of 150 to 350 °C (Table 1). Related to the Arrhenius assumption, lower activation energy provides a higher amount of branched isomers from *n*-hexane or cyclohexane isomerization. The values of E_a for *n*-hexane isomerization using P/HSi@BEA were 2 times lower than those for the N/HSi@BEA catalyst. However, when using cyclohexane as the reactant, N/HSi@BEA exhibited a slight reduction in the E_a value compared to

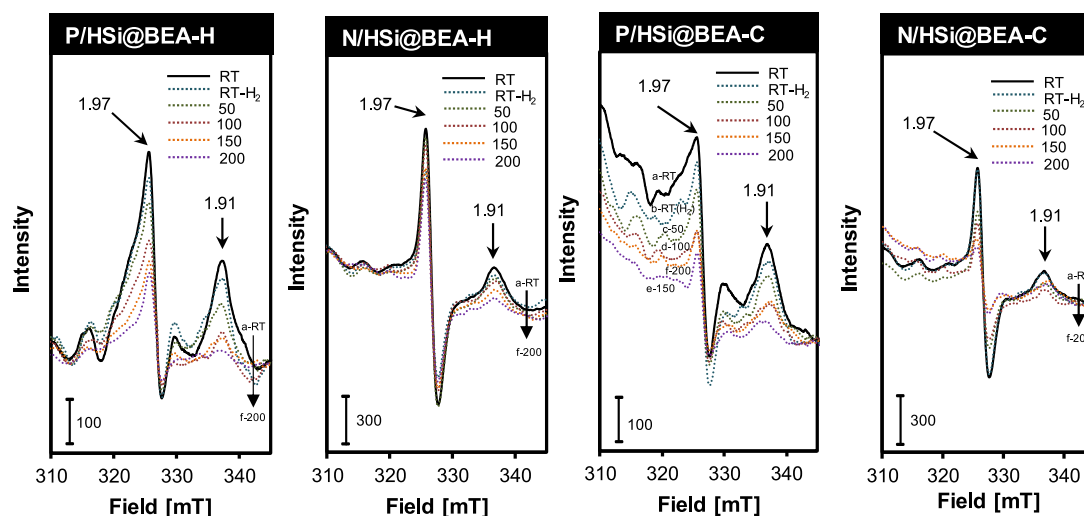


Figure 9. ESR spectra of P/HSi@BEA and N/HSi@BEA activated at 400 °C for 1 h, 50 Torr of preadsorbed *n*-hexane/cyclohexane at (a) room temperature (RT)-black color line, 100 Torr of hydrogen was adsorbed (b) room temperature (RT)-blue color dotted line, (c) 50 °C, green color dotted line; (d) 100 °C, red color dotted line; (e) 150 °C, orange color dotted line; (f) 200 °C, purple color dotted line. The preadsorbed *n*-hexane and cyclohexane were labeled as H and C, respectively.

the P/HSi@BEA catalyst. This different trend implied that the involvement of mesoporosity and the acidic sites concentration of the catalysts take a significant role in the reaction.

The effect of internal diffusional limitation of catalysts can be evaluated by applying the Weisz–Prater (NWP)⁷³ criterion as shown in Table 1. In summary, the presence of mesopores provides no diffusion limitation in the catalysts. The silica lamellar structure of HSi@BEA enhances the diffusion and accessibility of the reactants and products throughout the catalyst. It is also noted that the Weisz–Prater values are parallel with the above-mentioned results, where the phosphate group-type catalyst is favored for the straight chain reactant, while the nitrate group-type catalyst is more appropriate for the cyclic reactant.

In summary, the HSi@BEA catalyst loaded with the phosphate group provided much higher yields of branched isomers in *n*-hexane isomerization, while the nitrate group loaded on the HSi@BEA catalyst afforded greater yield in cyclohexane isomerization. The improvement in the active site accessibility and molecular transport in an environment of nonrestricted mesoporous channels clearly influences the enhancement of catalytic activity. Nevertheless, the fact that the augmentation in the yield of branched isomers is also associated with contributions from the strength of acidity of the catalysts could not be excluded. The moderate acidity with a high amount of Lewis acid sites from the P/HSi@BEA catalyst has provided a significant effect on increasing the yield or activity of straight chain hydrocarbon isomerization. Diversely, the high acidity character of the N/HSi@BEA catalyst was essential to contributing prominently in the cyclic hydrocarbon isomerization.⁷² Furthermore, the presence of electron acceptor Lewis acid sites in the catalysts was also accountable for the catalytic activity enhancement, as confirmed in the literature for numerous hydrocarbons.^{42,74–76} It was shown that the higher Lewis acid sites give greater generation of protonic acid sites during isomerization.^{42,77}

3.6. Dissociative Adsorption of Hydrogen Gas. Figure 9 displays the in situ ESR spectra of activated P/HSi@BEA and N/HSi@BEA catalysts with preadsorbed *n*-hexane or cyclohexane at room temperature up to 200 °C in a hydrogen

environment. ESR results can indirectly certify the ability of phosphate or nitrate groups in the generation of an electron from the formation of atomic hydrogen through dissociative adsorption of molecular hydrogen. Overall, the $(\text{PO}_x)^-(\text{H}_y)^+$ or $(\text{NO}_x)^-(\text{H}_y)^+$ was formed from the subsequent bonding of a proton with a P or N atom, respectively. The proton was generated by the loss of an electron from atomic hydrogen, followed by trapping the electron in the electron-deficient metal cations, which resulted in a reduction in the ESR signal at $g = 1.97$. The signal at $g = 1.97$ shows a significant decrease after being heated up to 200 °C in the presence of hydrogen for the preadsorbed *n*-hexane or cyclohexane of the P/HSi@BEA catalyst, indicating faster formation of an electron from hydrogen and being trapped in the electron-deficient metal cations. The N/HSi@BEA catalyst showed no significant changes in the signal intensity, demonstrating a lower electron formation from hydrogen and the electrons stuck in the electron-deficient metal cations. Higher generation of Lewis acid sites in the P/HSi@BEA catalyst, which is evident from Figure 8D, generates a large protonic acid site amount by alteration of the role of electron acceptors after dissociation of H_2 . As a result, a larger amount of protonic acid sites triggered the production of *n*-hexane isomers. Moreover, all catalysts also exhibited an additional two signals at $g = 1.91$ which relate to the vibration structure of nonbridging oxygen hole centers in silica or lattice defects present in both catalysts.⁷⁸ Both catalysts showed similar changes in the signal, which suggests that the lattice defects also play an insignificant role in the isomer formation of *n*-hexane and cyclohexane.

The promotive result of hydrogen can be distinct from the formation of protonic acid sites from the spillover of hydrogen from metal sites onto the catalyst support, which was reported by Hattori and co-workers.^{79,80} In addition, Iglesia and co-workers also have studied the hydrogen spillover effect on the zeolite as a support catalyst.⁸¹

4.0. CONCLUSION

P/HSi@BEA and N/HSi@BEA catalysts were prepared by impregnation of HSi@BEA with H_3PO_4 and HNO_3 , respectively. The catalysts' physical and chemical properties

were observed by XRD, N₂ physisorption, FESEM, TEM, ²⁷Al NMR, UV-DRS, FTIR, and ESR. The FESEM images revealed the preservation of the bicontinuous concentric lamellar morphology of HSi@BEA after the incorporation of phosphate and nitrate. XRD and ²⁷Al NMR results demonstrated that the impregnation of phosphate and nitrate led to extraction of Al from the catalyst framework. The N/HSi@BEA catalyst possessed the highest average pore diameter of 6.52 nm, followed by P/HSi@BEA and HSi@BEA catalysts. FTIR analysis confirmed that the existence of the P–OH species in the P/HSi@BEA catalyst reduced its acidity due to the weak acidic character of the species. However, the introduction of nitrate groups increases the catalyst acidity attributed to the Si(OH)Al formation as the Brønsted acid sites of the catalyst. Both catalysts displayed high interaction with hydrogen, as evident by the ESR analysis. However, ESR analysis showed that the dissociation of hydrogen to form protonic acid sites was faster for the P/HSi@BEA catalyst, and its Lewis acid sites influence the production of *n*-hexane isomers by playing the role of electron acceptor in generating the protonic acid sites. The mesoporosity of the N/HSi@BEA catalyst was found to play an essential role in enhancing the selective production of cyclohexane isomers. The phosphate group catalyst gave a higher yield of *n*-hexane isomers (50.3%), while the nitrate group catalyst contributed 48.4% of the cyclohexane isomers at 250 °C compared to the other catalysts. In this study, the P/HSi@BEA and N/HSi@BEA catalysts showed promising production of higher branched isomers for selective cyclic or noncyclic isomerization compared to the parent HSi@BEA and previous bare BEA catalysts.

■ ASSOCIATED CONTENT

SI Supporting Information

The Supporting Information is available free of charge at <https://pubs.acs.org/doi/10.1021/acs.inorgchem.9b02914>.

FESEM and EDX, ²⁷Al NMR, and FTIR analyses of some catalysts (PDF)

■ AUTHOR INFORMATION

Corresponding Author

Aishah Abdul Jalil – *Universiti Teknologi Malaysia, Johor, Malaysia*; orcid.org/0000-0003-0811-3168;
Phone: +60-7-5535581; Email: aishahaj@utm.my;
Fax: +60-7-5536165

Other Authors

Siti Maryam Izan – *Universiti Teknologi Malaysia, Johor, Malaysia*

Che Ku Nor Liana Che Ku Hitam – *Universiti Teknologi Malaysia, Johor, Malaysia*

Walid Nabgan – *Universiti Teknologi Malaysia, Johor, Malaysia*

Complete contact information is available at:
<https://pubs.acs.org/doi/10.1021/acs.inorgchem.9b02914>

Notes

The authors declare no competing financial interest.

■ ACKNOWLEDGMENTS

The authors gratefully acknowledge the financial support from the Universiti Teknologi Malaysia via Transdisciplinary

Research Grant (No. 06G52 and 06G53) and Ministry of Higher Education Malaysia through MyBrainSc Scholarship (Siti Maryam binti Izan).

■ REFERENCES

- (1) Hengsawad, T.; Srimingkwanchai, C.; Butnark, S.; Resasco, D. E.; Jongpatiwut. Effect of Metal-Acid Balance on Hydroprocessed Renewable Jet Fuel Synthesis from Hydrocracking and Hydroisomerization of Biohydrogenated Diesel over Pt-Supported Catalysts. *Ind. Eng. Chem. Res.* **2018**, *57*, 1429–1440.
- (2) Jaroszewska, K.; Masalska, A.; Czycz, D.; Grzechowiak, J. Activity of shaped Pt/ALSBA-15 catalysts in *n*-hexadecane hydroisomerization. *Fuel Process. Technol.* **2017**, *167*, 1–10.
- (3) Oya, S.; Kanno, D.; Watanabe, H.; Tamura, M.; Nakagawa, Y.; Tomishige, K. Catalytic Production of Branched Small Alkanes from Biohydrocarbons. *ChemSusChem* **2015**, *8*, 2472–2475.
- (4) Pastvova, J.; Pilar, R.; Moravkova, J.; Kaucy, D.; Rathousky, J.; Sklenak, S.; Sazama, P. Tailoring the Structure and Acid Site Accessibility of Mordenite Zeolite for Hydroisomerisation of *n*-hexane. *Appl. Catal., A* **2018**, *562*, 159–172.
- (5) Samad, J. E.; Blanchard, J.; Sayag, C.; Louis, C.; Regalbutto, J. R. The Controlled Synthesis of Metal-Acid Bifunctional Catalysts: The Effect of Metal: Acid Ratio and Metal-Acid Proximity in Pt Silica-Alumina Catalysts for *n*-Heptane Isomerization. *J. Catal.* **2016**, *342*, 203–212.
- (6) Pinto, T.; Arquillière, P.; Dufaud, V.; Lefebvre, F. Isomerization of *n*-hexane Over Pt-H₃PW₁₂O₄₀/SBA-15 Bifunctional Catalysts: Effect of The Preparation Method on Catalytic Performance. *Appl. Catal., A* **2016**, *528*, 44–51.
- (7) Liu, P.; Wu, M.; Wang, J.; Zhang, W.; Li, Y. Hydroisomerization of *n*-heptane over MoP/HB Catalyst Doped With Metal Additive. *Fuel Process. Technol.* **2015**, *131*, 311–316.
- (8) Guisnet, M. Ideal Bifunctional Catalysis Over Pt-Acid Zeolites. *Catal. Today* **2013**, *218–219*, 123–134.
- (9) Wang, Y.; Tao, Z.; Wu, B.; Xu, J.; Huo, C.; Li, K.; Chen, H.; Yang, Y.; Li, Y. Effect of Metal Precursors on the Performance of Pt/ZSM-22 Catalysts for *n*-hexadecane Hydroisomerization. *J. Catal.* **2015**, *322*, 1–13.
- (10) Fatah, N. A. A.; Triwahyono, S.; Jalil, A. A.; Ahmad, A.; Abdullah, T. A. T. *n*-Heptane Isomerization over Mesoporous Silica Nanoparticles (MSN): Dissociative-Adsorption of Molecular Hydrogen on Pt and Mo Sites. *Appl. Catal., A* **2016**, *516*, 135–143.
- (11) Li, W.; Zheng, J.; Luo, Y.; Tu, C.; Zhang, Y.; Da, Z. Hierarchical Zeolite Y with Full Crystallinity: Formation Mechanism and Catalytic Cracking Performance. *Energy Fuels* **2017**, *31*, 3804–3811.
- (12) Na, K.; Yoon, J.; Somorjai, G. A. Control of Model Catalytic Conversion Reaction Over Pt Nanoparticle Supported Mesoporous BEA Zeolite Catalysts. *Catal. Today* **2016**, *265*, 225–230.
- (13) Pastvova, J.; Kaucy, D.; Moravkova, J.; Rathousky, J.; Sklenak, S.; Vorokhta, M.; Brabec, L.; Pilar, R.; Jakubec, I.; Tabor, E.; Klein, P.; Sazama, P. Control of Model Catalytic Conversion Reaction Over Pt Nanoparticle Supported Mesoporous BEA Zeolite Catalysts. *ACS Catal.* **2017**, *7*, 5781–5795.
- (14) Baran, R.; Millot, Y.; Onfroy, T.; Krafft, J. M.; Dzwigaj, S. Influence of the Nitric Acid Treatment on Al Removal, Framework Composition and Acidity of BEA Zeolite Investigated by XRD, FTIR and NMR. *Microporous Mesoporous Mater.* **2012**, *163*, 122–130.
- (15) Li, W.; Zheng, J.; Luo, Y.; Da, Z. Effect of Hierarchical Porosity and Phosphorus Modification on the Catalytic Properties of Zeolite Y. *Appl. Surf. Sci.* **2016**, *382*, 302–308.
- (16) Hanafi, S. A.; Gobara, H. M.; Elmelawy, M. S.; Abo-El-Enein, S. A.; Alkahlawy, A. A. Catalytic Performance of Dealuminated H–Y Zeolite Supported Bimetallic Nanocatalysts in Hydroisomerization of *n*-Hexane and *n*-Heptane. *Egypt. J. Pet.* **2014**, *23*, 119–133.
- (17) Wang, Y.; Yokoi, T.; Namba, S.; Tatsumi, T. Effects of Dealumination and Desilication of Beta Zeolite on Catalytic Performance in *n*-Hexane Cracking. *Catalysts* **2016**, *6*, 8.

- (18) Najjar, H.; Zina, M. S.; Ghorbel, A. Study of the Effect of the Acid Dealumination on the Physico-Chemical Properties of Y Zeolite. *React. Kinet., Mech. Catal.* **2010**, *100*, 385–398.
- (19) Viswanadham, N.; Dixit, L.; Gupta, J. K.; Garg, M. O. Effect of Acidity and Porosity Changes of Dealuminated Mordenites on *n*-Hexane Isomerization. *J. Mol. Catal. A: Chem.* **2006**, *258*, 15–21.
- (20) Omegna, A.; Haouas, M.; Kogelbauer, A.; Prins, R. Realumination of Dealuminated HZSM-5 Zeolites By Acid Treatment: A Reexamination. *Microporous Mesoporous Mater.* **2001**, *46*, 177–184.
- (21) Silaghi, M. C.; Chizallet, C.; Sauer, J.; Raybaud, P. Dealumination Mechanisms of Zeolites and Extra-Framework Aluminum Confinement. *J. Catal.* **2016**, *339*, 242–255.
- (22) Xue, N.; Chen, X.; Nie, L.; Guo, X.; Ding, W.; Chen, Y.; Gu, M.; Xie, Z. Understanding the Enhancement of Catalytic Performance for Olefin Cracking: Hydrothermally Stable Acids in P/HZSM-5. *J. Catal.* **2007**, *248*, 20–28.
- (23) Liu, D.; Choi, W. C.; Lee, C. W.; Kang, N. Y.; Lee, Y. J.; Shin, C. H.; Park, Y. K. Steaming and Washing Effect of P/HZSM-5 in Catalytic Cracking of Naphtha. *Catal. Today* **2011**, *164*, 154–157.
- (24) Janardhan, H. L.; Shanbhag, G. V.; Halgeri, A. B. Shape-Selective Catalysis by Phosphate Modified ZSM-5: Generation of New Acid Sites With Pore Narrowing. *Appl. Catal., A* **2014**, *471*, 12–18.
- (25) Kaeding, W. W.; Butter, S. A. Production of Chemicals From Methanol. I. Low Molecular Weight Olefins. *J. Catal.* **1980**, *61*, 155–164.
- (26) Védrine, J. C.; Auroux, A.; Dejaive, P.; Ducarme, V.; Hoser, H.; Zhou, S. Catalytic and Physical Properties of Phosphorus-Modified ZSM-5 Zeolite. *J. Catal.* **1982**, *73*, 147–160.
- (27) Kolodziejski, W.; Fornés, V.; Corma, A. Solid-state NMR Study of Ultrastable Zeolite Y Modified With Orthophosphoric Acid. *Solid State Nucl. Magn. Reson.* **1993**, *2*, 121–129.
- (28) Corma, A.; Fornés, V.; Kolodziejski, W.; Martínez-Triguero, L. J. Orthophosphoric Acid Interactions with Ultrastable Zeolite Y: Infrared and NMR Studies. *J. Catal.* **1994**, *145*, 27–36.
- (29) Blasco, T.; Corma, A.; Martínez-Triguero, J. Hydrothermal Stabilization of ZSM-5 Catalytic-Cracking Additives by Phosphorus Addition. *J. Catal.* **2006**, *237*, 267–277.
- (30) Ramesh, K.; Jie, C.; Han, Y. F.; Borgna, A. Synthesis, characterization, and catalytic activity of phosphorus modified H-ZSM-5 catalysts in selective ethanol dehydration. *Ind. Eng. Chem. Res.* **2010**, *49*, 4080–4090.
- (31) Caro, J.; Bülow, M.; Derewinski, M.; Haber, J.; Hunger, M.; Kärger, J.; Pfeifer, H.; Storek, W.; Zibrowius, B. NMR and IR Studies of Zeolite H-ZSM-5 Modified with Orthophosphoric Acid. *J. Catal.* **1990**, *124*, 367–375.
- (32) Seo, G.; Ryoo, R. ³¹P, ²⁷Al, and ¹²⁹Xe NMR study of Phosphorus-Impregnated HZSM-5 Zeolite Catalysts. *J. Catal.* **1990**, *124*, 224–230.
- (33) Lischke, G.; Eckelt, R.; Jerschke, H. G.; Parlitz, B.; Schreier, E.; Storek, W.; Zibrowius, B.; Öhlmann, G. Spectroscopic and Physicochemical Characterization of P-Modified H-ZSM-5. *J. Catal.* **1991**, *132*, 229–243.
- (34) Teh, L.P.; Triwahyono, S.; Jalil, A.A.; Firmansyah, M.L.; Mamat, C.R.; Majid, Z.A. Fibrous Silica Mesoporous ZSM-5 For Carbon Monoxide Methanation. *Appl. Catal., A* **2016**, *523*, 200–208.
- (35) Szostak, R.; *Handbook of Molecular Sieves [Internet]*, 1st ed.; Springer: Netherlands, 1992; p 584.
- (36) Higgins, J. B.; LaPierre, R. B.; Schlenker, J. L.; Rohrman, A. C.; Wood, J. D.; Kerr, G. T.; Rohrbaugh, W. J. The Framework of Zeolite Beta. *Zeolites* **1988**, *8*, 446–452.
- (37) Wang, W.; Zhang, W.; Chen, Y.; Wen, X.; Li, H.; Yuan, D.; Guo, Q.; Ren, S.; Pang, X.; Shen, B. Mild-acid-assisted Thermal or Hydrothermal Dealumination of Zeolite Beta, Its Regulation to Al Distribution and Catalytic Cracking Performance to Hydrocarbons. *J. Catal.* **2018**, *362*, 94–105.
- (38) Dzwigaj, S.; Popovych, N.; Kyriienko, P.; Krafft, J.-M.; Soloviev, S. Incorporation of Silver Atoms into the Vacant T - Atom Sites of the Framework of SiBEA Zeolite as Mononuclear Ag (I) Evidenced by XRD. *Microporous Mesoporous Mater.* **2013**, *182*, 16–24.
- (39) Yan, Z.; Ma, D.; Zhuang, J.; Liu, X.; Liu, X.; Han, X.; Bao, X.; Chang, F.; Xu, L.; Liu, Z. On the Acid-Dealumination of USY Zeolite: A Solid State NMR Investigation. *J. Mol. Catal. A: Chem.* **2003**, *194*, 153–167.
- (40) Gou, M.; Wang, R.; Qiao, Q.; Yang, X. Effect of Phosphorus on Acidity and Performance of HZSM-5 for the Isomerization of Styrene Oxide to Phenylacetaldehyde. *Appl. Catal., A* **2014**, *482*, 1–7.
- (41) Zhao, G.; Xie, Z.; Jin, W.; Yang, W.; Chen, Q.; Tang, Y. Effect of Phosphorus on HZSM-5 Catalyst for C4-Olefin Cracking Reactions to Produce Propylene. *J. Catal.* **2007**, *248*, 29–37.
- (42) Izan, S. M.; Triwahyono, S.; Jalil, A. A.; Majid, Z. A.; Fatah, N. A. A.; Hamid, M. Y. S.; Ibrahim, M. Additional Lewis Acid Sites of Protonated Fibrous Silica BEA Zeolite (HSi@BEA) Improving the Generation of Protonic Acid Sites in the Isomerization of C6 Alkane and Cycloalkanes. *Appl. Catal., A* **2019**, *570*, 228–37.
- (43) Mustapha, F. H.; Jalil, A. A.; Mohamed, M.; Triwahyono, S.; Hassan, N. S.; Khusnun, N. F.; Hitam, C. N. C.; Rahman, A. F. A.; Firmansyah, L.; Zolkifli, A. S. New Insight Into Self-Modified Surfaces With Defect-Rich Rutile TiO₂ as a Visible-Light-Driven Photocatalyst. *J. Cleaner Prod.* **2017**, *168*, 1150–1162.
- (44) Yao, W.; Chen, Y.; Min, L.; Fang, H.; Yan, Z.; Wang, H.; Wang, J. Liquid Oxidation of Cyclohexane to Cyclohexanol over Cerium-Doped MCM-41. *J. Mol. Catal. A: Chem.* **2006**, *246*, 162–166.
- (45) Fatah, N. A. A.; Triwahyono, S.; Jalil, A. A.; Ahmad, A.; Abdullah, T. A. T. *n*-Heptane Isomerization Over Mesoporous Silica Nanoparticles (MSN): Dissociative-Adsorption of Molecular Hydrogen on Pt and Mo Sites. *Appl. Catal., A* **2016**, *516*, 135–143.
- (46) Abdul Jalil, A.; Zolkifli, A. S.; Triwahyono, S.; Abdul Rahman, A. F.; Mohd Ghani, N. N.; Shahul Hamid, M. Y.; Mustapha, F. H.; Izan, S. M.; Nabgan, B.; Ripin, A. Altering Dendrimer Structure of Fibrous-Silica-HZSM-5 for Enhanced Product Selectivity of Benzene Methylation. *Ind. Eng. Chem. Res.* **2019**, *58*, 553–562.
- (47) Chlebda, D. K.; Stachurska, P.; Jedrzejczyk, R. J.; Kuteraskinski, L.; Dziedzicka, A.; Gorecka, S.; Chmielarz, L.; Lojewska, J.; Sitarz, M.; Jodlowski, P. DeNO_x Abatement over Sonically Prepared Iron-Substituted Y, USY and MFI Zeolite Catalysts in Lean Exhaust Gas Conditions. *Nanomaterials* **2018**, *8*, 21.
- (48) Zanjanchi, M. A.; Ghanadzadeh, A.; Khadem-Nahvi, F. Incorporation of Silicon into AIPO-5 Framework Sites: Higher Thermal Stability and Lower Extra-Framework Aluminum Concentration. *J. Inclusion Phenom. Mol. Recognit. Chem.* **2002**, *42*, 295–299.
- (49) Zhang, Y.; Liu, D.; Men, Z.; Huang, K.; Lv, Y.; Li, M.; Lou, B. Hydroisomerization of *n*-dodecane over Bi-Porous Pt-Containing Bifunctional Catalysts: Effects of Alkene Intermediates' Journey Distances within the Zeolite Micropores. *Fuel* **2019**, *236*, 428–436.
- (50) Erdogan, B.; Arbag, H.; Yasyerli, N. SBA-15 Supported Mesoporous Ni and Co Catalysts with High Coke Resistance for Dry Reforming of Methane. *Int. J. Hydrogen Energy* **2018**, *43*, 1396–1405.
- (51) Ma, Z.; Meng, X.; Liu, N.; Shi, L. Pd-Ni Doped Sulfated Zirconia: Study of Hydrogen Spillover and Isomerization of *n*-Hexane. *Mol. Catal.* **2018**, *449*, 114–121.
- (52) Hitam, C. N. C.; Jalil, A. A.; Triwahyono, S.; Ahmad, A.; Jaafar, N. F.; Salamun, N.; Fatah, N. A. A.; Teh, L. P.; Khusnun, N. F.; Ghazali, Z. Synergistic Interactions of Cu and N on Surface Altered Amorphous TiO₂ Nanoparticles for Enhanced Photocatalytic Oxidative Desulfurization of Dibenzothiophene. *RSC Adv.* **2016**, *6*, 76259–76268.
- (53) Lyu, J.; Hu, H.; Tait, C.; Rui, J.; Lou, C.; Wang, Q.; Han, W.; Zhang, Q.; Pan, Z.; Li, X. Benzene Alkylation with Methanol over Phosphate Modified Hierarchical Porous ZSM-5 with Tailored Acidity. *Chin. J. Chem. Eng.* **2017**, *25*, 1187–1194.
- (54) Sazama, P.; Kaucy, D.; Moravkova, J.; Pilar, R.; Klein, P.; Pastvova, J.; Tabor, E.; Sklenak, S.; Jakubec, I.; Mokrzycki, L. Superior Activity of Non-Interacting Close Acidic Protons in Al-Rich Pt/H-*BEA Zeolite in Isomerization of *n*-Hexane. *Appl. Catal., A* **2017**, *533*, 28–37.

- (55) Ghani, N. N. M.; Jalil, A. A.; Triwahyono, S.; Aziz, M. A. A.; Rahman, A. F. A.; Hamid, M. Y. S.; Izan, S. M.; Nawawi, M. G. M. Tailored Mesoporosity and Acidity of Shape-Selective Fibrous Silica Beta Zeolite for Enhanced Toluene Co-Reaction with Methanol. *Chem. Eng. Sci.* **2019**, *193*, 217–229.
- (56) Fathi, S.; Sohrabi, M.; Falamaki, C. Improvement of HZSM-5 Performance by Alkaline Treatments: Comparative Catalytic Study in the MTG Reactions. *Fuel* **2014**, *116*, 529–537.
- (57) Mobasherpour, I.; Heshajin, M. S.; Kazemzadeh, A.; Zakeri, M. J. Synthesis of Nanocrystalline Hydroxyapatite by using Precipitation Method. *J. Alloys Compd.* **2007**, *430*, 330–333.
- (58) Gu, C.; Katti, D. R.; Katti, K. S. Molecular and Biomolecular Spectroscopy Photoacoustic FTIR Spectroscopic Study of Undisturbed Human Cortical Bone. *Spectrochim. Acta, Part A* **2013**, *103*, 25–37.
- (59) Hakiri, R.; Ameer, I.; Abid, S.; Derbel, N. Synthesis, X-Ray Structural, Hirshfeld Surface Analysis, FTIR, MEP and NBO Analysis using DFT Study of a 4-Chlorobenzylammonium Nitrate $(C_7ClH_9N)^+(NO_3)^-$. *J. Mol. Struct.* **2018**, *1164*, 486–492.
- (60) Marques, J. P.; Gener, I.; Ayrault, P.; Lopes, J. M.; Ramôa Ribeiro, F.; Guisnet, M. Semi-Quantitative Estimation by IR of Framework, Extraframework and Defect Al Species of HBEA Zeolites. *Chem. Commun.* **2004**, *10*, 2290–2291.
- (61) Sammoury, H.; Toufaily, J.; Cherry, K.; Hamieh, T.; Pouilloux, Y.; Pinard, L. Desilication of *BEA Zeolites using Different Alkaline Media: Impact on Catalytic Cracking of *n*-Hexane. *Microporous Mesoporous Mater.* **2018**, *267*, 150–163.
- (62) Jusoh, N. W. C.; Jalil, A. A.; Triwahyono, S.; Mamat, C. R. Tailoring the Metal Introduction Sequence onto Mesoporous Silica Nanoparticles Framework: Effect on Physicochemical Properties and Photoactivity. *Appl. Catal., A* **2015**, *492*, 169–176.
- (63) Jusoh, N. W. C.; Jalil, A. A.; Triwahyono, S.; Karim, A. H.; Salleh, N. F.; Annuar, N. H. R.; Jaafar, N. F.; Firmansyah, M. L.; Mukti, R. R.; Ali, M. W. Structural Rearrangement of Mesoporous Silica Nanoparticles Incorporated with ZnO Catalyst and Its Photoactivity: Effect of Alkaline Aqueous Electrolyte Concentration. *Appl. Surf. Sci.* **2015**, *330*, 10–19.
- (64) Najjar, H.; Zina, M. S.; Ghorbel, A. The Effect of Extra Framework Species and Acid Properties of Dealuminated Zeolitic Support on the Catalytic Behavior of Palladium in *n*-Hexane Isomerization Reaction. *React. Kinet., Mech. Catal.* **2014**, *111*, 775–790.
- (65) He, M.-Y.; Peng, L.; Xue, N.; Ding, J.; Wang, M.; Wang, Y. Combined Desilication and Phosphorus Modification for High-Silica ZSM-5 Zeolite with Related Study of Hydrocarbon Cracking Performance. *Appl. Catal., A* **2015**, *503*, 147–155.
- (66) Tang, Y.; Shen, W.; Yue, Y.; Liu, J.; Shen, Z.; Zhang, C.; Hua, W.; Xu, H. Methanol to Propylene: Effect of Phosphorus on a High Silica HZSM-5 Catalyst. *Catal. Commun.* **2009**, *10*, 1506–1509.
- (67) Van Der Bij, H. E.; Weckhuysen, B. M. Phosphorus Promotion and Poisoning in Zeolite-Based Materials: Synthesis, Characterisation and Catalysis. *Chem. Soc. Rev.* **2015**, *44*, 7406–7428.
- (68) Sazegar, M. R.; Mahmoudian, S.; Mahmoudi, A.; Triwahyono, S.; Jalil, A. A.; Mukti, R. R.; Nazirah Kamarudin, N. H.; Ghoreishi, M. K. Catalyzed Claisen–Schmidt Reaction by Protonated Aluminate Mesoporous Silica Nanomaterial Focused on the (E)-Chalcone Synthesis as a Biologically Active Compound. *RSC Adv.* **2016**, *6*, 11023–11031.
- (69) Van Der Bij, H. E.; Cicmil, D.; Wang, J.; Meirer, F.; de Groot, F. M. F.; Weckhuysen, B. M. Aluminum-Phosphate Binder Formation in Zeolites as Probed with X-ray Absorption Microscopy. *J. Am. Chem. Soc.* **2014**, *136* (51), 17774–17787.
- (70) Ogoshi, T.; Sueto, R.; Yoshikoshi, K.; Yamagishi, T. One-dimensional Channels Constructed from Per-Hydroxylated Pillar[6]-Arene Molecules for Gas and Vapour Adsorption. *Chem. Commun.* **2014**, *50*, 15209–15211.
- (71) D'Ippolito, S. A.; Pirault-Roy, L.; Especel, C.; Epron, F.; Pieck, C. L. Influence of Support Acidity and Ir Content on the Selective Ring Opening of Decalin over Ir/SiO₂-Al₂O₃. *RSC Adv.* **2017**, *7*, 46803–46811.
- (72) Arribas, M. A.; Martinez, A. The Influence of Zeolite Acidity for the Coupled Hydrogenation and Ring Opening of 1-Methylnaphthalene on Pt/USY Catalysts. *Appl. Catal., A* **2002**, *230*, 203–217.
- (73) Weisz, P. B.; Prater, C. D. J. Interpretation of Measurements in Experimental Catalysis. *Adv. Catal.* **1954**, *6*, 143–196.
- (74) Setiabudi, H. D.; Jalil, A. A.; Triwahyono, S. Ir/Pt-HZSM5 for *n*-pentane Isomerization: Effect of Iridium Loading on the Properties and Catalytic Activity. *J. Catal.* **2012**, *294*, 128–135.
- (75) Fatah, N. A. A.; Triwahyono, S.; Jalil, A. A.; Salamun, N.; Mamat, C. R.; Majid, Z. A. *n*-Heptane Isomerization over Molybdenum Supported on Bicontinuous Concentric Lamellar Silica KCC-1: Influence of Phosphorus and Optimization using Response Surface Methodology (RSM). *Chem. Eng. J.* **2017**, *314*, 650–659.
- (76) Lewis, E. A.; Marcinkowski, M. D.; Murphy, C. J.; Liriano, M. L.; Sykes, E. C. H. Hydrogen Dissociation, Spillover, and Desorption from Cu-Supported Co Nanoparticles. *J. Phys. Chem. Lett.* **2014**, *5*, 3380–3385.
- (77) Triwahyono, S.; Jalil, A. A.; Musthofa, M. Generation of Protonic Acid Sites from Pentane on the Surfaces of Pt/SO₄²⁻-ZrO₂ And Zn/H-ZSM5 Evidenced by IR Study of Adsorbed Pyridine. *Appl. Catal., A* **2010**, *372*, 90–93.
- (78) Hussain, I.; Jalil, A. A.; Mamat, C. R.; Siang, T. J.; Rahman, A. F. A.; Azami, M. S.; Adnan, R. H. New Insights on the Effect of the H₂/CO ratio for enhancement of CO methanation over Metal-free Fibrous Silica ZSM-5: Thermodynamic and Mechanistic Studies. *Energy Convers. Manage.* **2019**, *199*, 112056.
- (79) Hattori, H.; Shishido, T. Molecular Hydrogen-originated Protonic Acid Site as Active Site on Solid Acid Catalyst. *Catal. Surv. Jpn.* **1997**, *1*, 205–13.
- (80) Hattori, H. Molecular Hydrogen-Originated Protonic Acid Site. *Stud. Surf. Sci. Catal.* **2001**, *138*, 3–12.
- (81) Iglesia, E. Bifunctional Pathways in Catalysis by Solid Acids and Bases. *Catal. Today* **1997**, *38*, 339–360.